

A facile approach to fabricate highly sensitive, flexible strain sensor based on elastomeric/graphene platelet composite film

Meng, Q., Liu, Z., Sen, H. & Cai, R.

Author post-print (accepted) deposited by Coventry University's Repository

Original citation & hyperlink: Meng, Qingshi et al. "A facile approach to fabricate highly sensitive, flexible strain sensor based on elastomeric/graphene platelet composite film". *Journal of Materials Science*. 2019, 54(15). 10856–10870.

<https://doi.org/10.1007/s10853-019-03650-1>

DOI 10.1007/s10853-019-03650-1

ISSN 0022-2461

ESSN 1573-4803

Publisher: Springer

The final publication is available at Springer via <http://dx.doi.org/10.1007/s10853-019-03650-1>

Copyright © and Moral Rights are retained by the author(s) and/ or other copyright owners. A copy can be downloaded for personal non-commercial research or study, without prior permission or charge. This item cannot be reproduced or quoted extensively from without first obtaining permission in writing from the copyright holder(s). The content must not be changed in any way or sold commercially in any format or medium without the formal permission of the copyright holders.

This document is the author's post-print version, incorporating any revisions agreed during the peer-review process. Some differences between the published version and this version may remain and you are advised to consult the published version if you wish to cite from it.

A facile approach to fabricate highly sensitive, flexible strain sensor based on elastomeric/graphene platelets composite film

Qingshi Meng^{a*}, Zhiwen Liu^a, Sensen Han^a, Lisheng Xu^b, Sherif Araby^{c,d}, Rui Cai^e,
Yu Zhao^a, Shaowei Lu^{a*}, Tianqing Liu^f

^a College of Aerospace Engineering, Shenyang Aerospace University (SAU), Shenyang, 110136, China

^b School of Sino-Dutch Biomedical and Information Engineering, Northeastern University, Shenyang 110819, Liaoning, China

^c College of Engineering and Technology, American University of the Middle East, Kuwait

^d Department of Mechanical Engineering, Benha Faculty of Engineering, Benha University, Egypt

^e School of Mechanical, Aerospace and Automotive Engineering, Coventry University, Coventry, UK

^f QIMR Berghofer Medical Research Institute, Brisbane Queensland, 4006, Australia

*Corresponding Authors: Qingshi Meng and Shaowei Lu;

Emails: mengqingshi@hotmail.com (Q. Meng) and lushaowei_2005@163.com (S. Lu)

Abstract

This work developed a facile approach to fabricate highly sensitive and flexible polyurethane/graphene platelets composite film for wearable strain sensor. The composite film was fabricated via layer by layer laminating method which is simple and cost-effective; it exhibited outstanding electrical conductivity of 1430 ± 50 S/cm and high sensitivity to strain (the gauge factor is up to 150). In the sensor application test, the flexible strain sensor achieves real-time monitoring accurately for five bio-signals such as pulse movement, finger movement, cheek movement, etc. giving a great potential as wearable-sensing device. In addition, the developed strain sensor shows response to pressure and temperature in a certain region. A multifaceted comparison between reported flexible strain sensors and our strain sensor was made highlighting the advantages of the current work in terms (1) high sensitivity (gauge factor) and flexibility, (2) facile approach of fabrication, and (3) accurate monitoring for body motions.

Key words: Graphene; Composite films; Electrical conductivity; Strain sensor; Wearable.

1. Introduction

Within the last two decades, strain sensors were widely used in various fields and applications, such as aerospace, automotive, construction, biomedical and other new energy fields [1-5]. Since strain sensor has the ability to detect mechanical deformations due to external loads, it has attracted considerable interests for various wearable devices to transform human physical motion to electric signals for disease diagnosis, therapy and health conditions monitoring [6-10]. In most cases, strain sensor is based on piezo-resistance theory in which mechanical deformations translate into resistance changes by strain gauge and finally monitored by electric signal. *At present, the commonly used strain sensors are made of rigid materials such as copper-nickel and nichrome alloy. These types of strain sensors are accurate in measurement, reliable and produced in largescale. However, their main drawbacks that they made of rigid the materials featuring low gauge factor and hence low sensitivity. Thus, they are not able to detect large deformation on complex curve surface or monitor body motions as a wearable device. The strain sensor based on flexible-conductive composites must possess high flexibility and gauge factor, and able to detect small to large strain deformations.*

There are various conductive nanomaterials including metals (gold nanoparticle, gold and silver nanowires) and carbon-based nanomaterials such as carbon blacks (CBs) and carbon nanotubes (CNTs), which have been extensively studied in developing flexible strain sensors [11-16]. Although metal-based nanomaterials are stable, most of them are costly and poorly stretchable, and they are susceptible to oxidization when they are used in wearable devices [17, 18]. CBs and CNTs show advantages of light weight and desirable sensitivity, but they also have limitations; CB based polymer composites shows relatively low electrical conductivity due to its low dimensionality (aspect ratio) which is detrimental to strain sensor, and CB has harmful effect on human health [19-21]. Single-walled carbon nanotubes (SWCNTs) have fascinating properties in strain gauging performances and conductivity, but high cost and difficulty in large-scale industrial production limit their application. Multi-walled carbon nanotubes (MWCNTs) are relatively cheaper with similar properties. However, both of them are not favorable in developing thin-films composite due to their highly entangled structure [17, 22-24]. Therefore, it is a formidable challenge to select novel conductive materials for fabrication of highly stretchable and flexible strain sensors.

Graphene has attracted enormous interest in fabrication of flexible strain sensors due to its exceptional properties—Young's modulus 1 TPa, tensile strength 130 GPa, stretch-ability up to 25% and electrical conductivity 6000 S/cm [25, 26]. Pristine graphene and graphene fabricated by CVD are not cost-effective with poor reproducibility and controllability for size dimension [27]. *Graphene oxide and reduced graphene oxide [28] are other derivatives of graphene; their fabrication process needs strong acids and large quantities of other chemicals. Fabrication process takes dozens of hours as well as the yield is not scalable [29]. Additionally, it is limited by low structural integrity implying unsatisfactory electrical conductivity [30].* More recently, graphene platelets (GnPs) have been reported to demonstrate the following advantages (i) high electrical conductivity of 1460 S/cm, (ii) each platelet being 3 nm in thickness, offering sufficient interface for stress and electron transfer in composites, and (iii) cost-effectiveness (\$20/kg) [31-35]. *Polyurethane (PU) is a multi-purpose polymer with the advantage of tailoring to meet demands; it can be molded in various forms including foams, thermoplastic elastomers, adhesives and paintings. PU-nanofiller composites have been reported in plethora studies to improve mechanical performance [36, 37], and functional properties such as hydrophilicity [37], electrical conductivity [37], and piezoresistivity's sensibility [38, 39].*

Developing nanofiller-based sensors to detect numerous signals including—but not limited—mechanical strain, temperature change [40, 41], and pressure change [42] using nanofillers is an interest for both academia and industry. For example; Tang's group has investigated polyurethane/graphene oxide composite as multifunctional sensors to detect flame [40, 41] and organic vapor sensing [43]. Herein, we developed a flexible, highly sensitive and electrically conductive polyurethane (PU)/GnP composite film fabricated by a facile approach for wearable strain sensor. *The flexible strain sensor has a similar sandwich structure with the traditional strain sensor.* The PU film was used as substrate with the advantage of excellent elasticity, ultra-light weight and non-toxicity. The PU/GnP thin-film was used as strain gauge in a strain sensor system. The PU/GnP composite film demonstrates excellent electrical conductivity (1430 ± 50 S/cm) and high sensitivity (gauge factor up to 150), demonstrating high potential as a flexible strain sensor. It is as wearable strain sensor device achieving accurate monitoring for body motions such as pulse movement, cheek movement, and forearm muscle movement, etc. Comparing with the previously demonstrated flexible strain sensor, our sensor

realized accurate real-time monitoring for both low and high frequency body motions. *Additionally, since fabrication of GnPs is simple and scalable compared to graphene oxide, our strain PU/GnP strain sensor has high potential in commercialization.*

2. Experimental Section:

2.1 Materials:

The graphite intercalation compound (*GIC Asbury 1395*) was kindly supplied by *Asbury Carbons*, NJ, USA. *The elastomer that was used in this study is polyurethane (PU). A PU film –0.04mm in thickness–* was purchased from local market which is widely used in medical treatment and leather industry. Acrylics pressure-sensitive adhesive was provided by *Shuhua Hengsheng* chemical company, Sichuan, China.

2.2 Fabrication of graphene platelets

GnPs were prepared by a published method [44]. In brief, the fabrication of GnPs is thermally expanding a commercial graphite intercalation compound in a crucible at 700°C for 1 min. The thermal expansion converted the compounds into worm-like structure which is delaminated by ultrasonication for 2h in acetone (under 20°C); then GnPs were produced after drying them in the oven overnight [30, 45].

2.3 Fabrication of GnP film

A glass mold was designed to load GnPs, and then pressed them using two metal sheets with smooth surface to make GnPs into primary rectangular shape with uniform thickness. Followed by further pressing the film using a hydraulic press for 1 min under 1 MPa pressure to form a thin GnP film. As shown in Fig. 1, this GnP film has good surface integrity, desirable flexibility and uniform thickness.

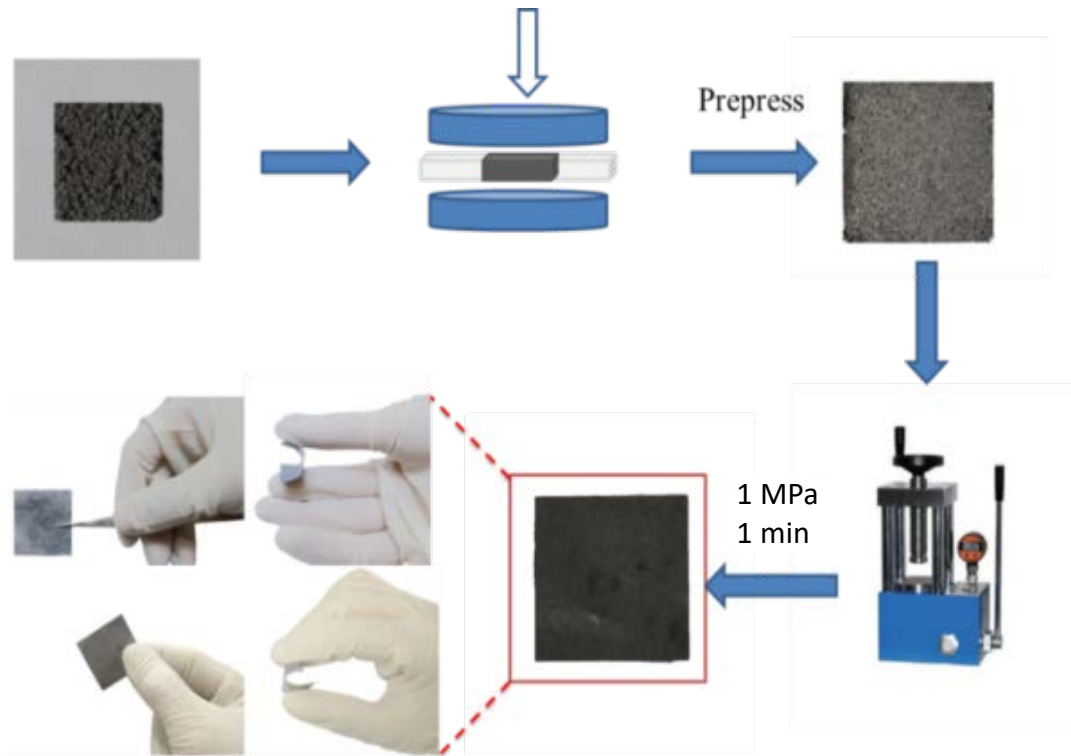


Fig. 1. Schematic illustrates the fabrication procedures of graphene platelets film with digital images for the prepared film.

2.4 Fabrications of strain sensor

Fig. 2 illustrates the schematic of fabrication of strain sensor based on PU/GnP composite film. The sensor was assembled on an ultra-thin PU film. *First, a acrylics pressure-sensitive adhesive was smeared over ultra-thin PU film (image a); then placed a GnP film at the center area of the PU film (image b). An isotropic conductive adhesive (ICA) was painted at both ends of the GnP film connected to copper wires (image b). Another PU film with acrylics pressure-sensitive adhesive covered the top of the GnP film (image c). Finally, the composite film was pressed by the hydraulic press at 1 MPa for 1 min (image C). Eventually, a PU-GnP-PU sandwich is used as strain sensor (image d).*

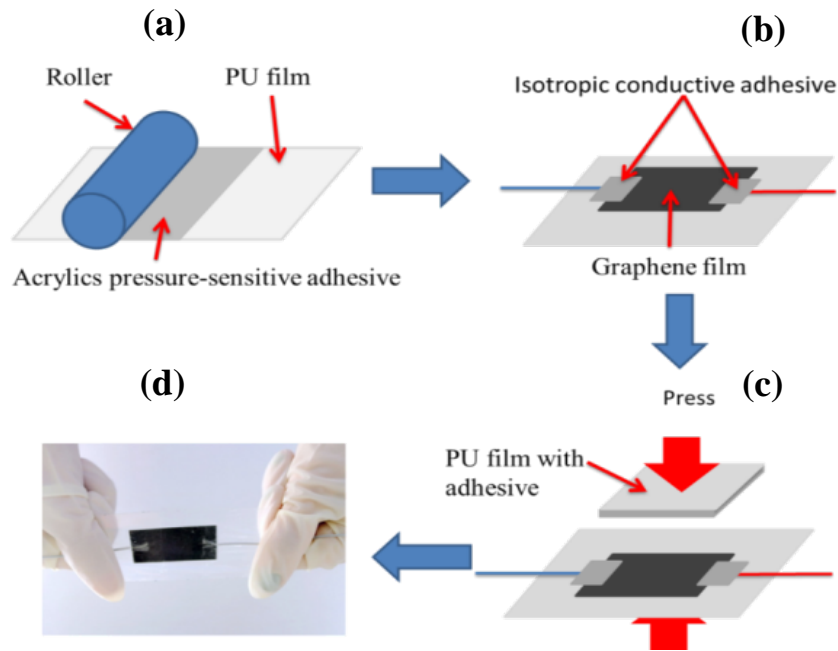


Fig. 2. Schematic illustrations of the fabrication of strain sensor with digital photograph of strain sensor prepared.

The average thicknesses of PU film and acrylics pressure-sensitive adhesive (APSA) are 0.04 ± 0.003 mm and ~ 0.01 mm, respectively. The thickness of GnP film depends on the weight of GnPs. The thickness of assembled composite film is equal to the sum of thickness of GnP film, PU film and Acrylics pressure-sensitive adhesive layer. Table 1 lists the specification of all the prepared GnP composite films.

Table 1. The specification of GnP composite films

Samples	Weight of GnPs (g)	Thickness of GnP film (mm)	Thickness of GnP composite film (mm)	Film size (mm)
1	0	0	0.1	40×40
2	0.040 ± 0.005	0.02 ± 0.003	0.12	40×40
3	0.082 ± 0.005	0.05 ± 0.003	0.15	40×40
4	0.115 ± 0.005	0.07 ± 0.003	0.17	40×40
5	0.165 ± 0.005	0.10 ± 0.003	0.20	40×40

2.5 Characterization

Scanning electron microscope (SEM) was conducted using a SEM (JEOL JSM-7800F) at 5 kV accelerating voltage. It was used to present images for the composite films' cross section and surface. The high-magnification transmission electron microscope (TEM) images were taken from a JEOL microscope operated at 120kV.

Mechanical properties were measured using Instron tensile testing machine at a cross-head speed of 2 mm/min at room temperature (25°C). Young's modulus and tensile strength of the samples were determined from the obtained stress-strain curves.

The sensitivity of the strain sensor is represented by the gauge factor (GF), that is, the ratio of the changes in relative electrical resistance to the applied tensile strain. In order to investigate the sensitivity of the strain sensor, the GF of the composite films is calculated using the following equation:

$$GF = \frac{\Delta R/R_0}{\Delta L/L_0} = \frac{\Delta R/R_0}{\varepsilon} \quad \text{Eq.1}$$

where R_0 is the initial resistance of the sensor, ΔR is the relative resistance change under deformation, L_0 is the initial length of the sensor, and ΔL is the relative elongation of the film in the axial direction, and ε is the strain [46]. The strain was collected by Instron tensile machine at speed of 2mm/min. FLUKE data acquisition unit was used to measure the electrical resistance of the strain sensor simultaneously with tensile testing was running; then the GF was calculated according to the equation.

In the sensor applications section, the flexible strain sensor was glued on the skin surface and the FLUKE data acquisition unit was used to measure the resistance of the flexible strain sensor. Similarly, the temperature and pressure responses were performed using the FLUKE data acquisition unit to record the resistance of flexible strain sensor under different pressure and temperature conditions. Program-controlled temperature furnace was used to control the temperature of the sensor from 20 to 150°C at heating rate 1°C /min. The hydraulic press was used to apply pressure on the sensor from 0 to 1000 kPa at room temperature (25 °C).

3. Results and discussion

3.1 Characterization of graphene platelets (GnPs)

Fig. 3a illustrates high-resolution TEM micrographs of a typical GnP sheet. The ordered lines suggest the GnP sheet has intact crystalline structures. These crystalline structures could create high electrical conductivity of GnP. This highly crystalline structure is in agreement with the x-ray photoelectron spectroscopy (XPS) analysis (Fig. 3b) which showed the C/O ratio is nearly 13.2 for GnPs. Thus, our GnPs would be a promising precursor for the fabrication of highly conductive sensors.

In Fig. 3c, GnPs lead to obvious absorptions at 1340 cm^{-1} , 1585 cm^{-1} and 2690 cm^{-1} which correspond to D, G, and 2D bands, respectively. G band refers to sp^2 resonance on an ordered graphitic lattice, while D band is activated from the first-order scattering process of sp^2 carbons by the presence of in-plane substitutional hetero-atoms, vacancies, grain boundaries or other defects, which might be sp^3 hybridized carbon structure associating with the quantity of impurity or oxidation degree. Since all samples were tested in the powder form, there is no point to discuss 2D band. The D- to G-band ratio of GnPs ($I_D/I_G = 0.07$) is much lower than those of other graphene derivates and graphite [30, 47], revealing a far better structural integrity in case of our GnPs. These results also align with TEM and XPS analysis.

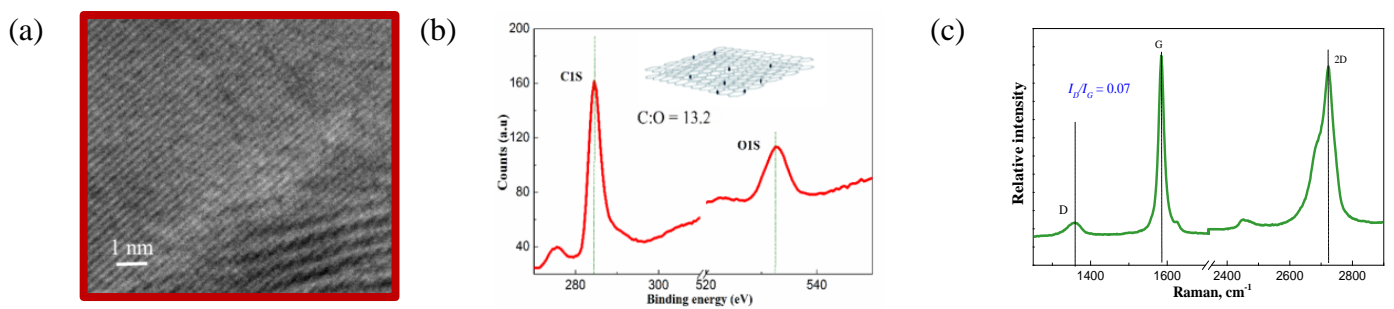


Fig. 3 Morphology of graphene platelets: (a) high-resolution TEM image, (b) XPS analysis and (c) Raman spectra

3.2 Morphology of PU/GnP composite film

Each of our GnP contains 1–4 layers of graphene sheets as reported previously [44, 45]. The GnP film was fabricated by pressing powder of GnPs forming a 2D-overlap GnP film (illustrated in Fig. 2). Then, following the procedures mentioned in Section 2.4, a PU/GnP composite film was fabricated. A cross-section of PU/GnP composite film of 0.17 mm in thickness was investigated using SEM imaging. Fig. 4a shows the cross-sectional morphology of the composite film. The composite film shows a layered structure which consists of GnP film, acrylics pressure-sensitive adhesive (APSA) and PU layers. As shown in images b&c (Fig. 4), GnPs are tightly stacked and overlapped after pressing to form global conductive network. At high magnification, images d–f shows the surface morphology of the GnP film, Fig. 4e demonstrates the film has good surface integrity; Fig. 4d shows the connections and overlaps between adjacent platelets creating plenty of conductive paths. Fig. 4f shows the micro-sized cracks and pores contained in the GnP film. Stress, strain, vibration and other deformations cause the changes of conductive network resulting in dramatic resistance change mainly attributed to three mechanisms: (1) tunneling resistance change between adjacent platelets due

to the expansion of micro-cracks, (2) influence of geometrical changes of GnP films, and (3) piezo-resistance of individual GnPs due to deformation upon loading [48]. The Schematic in Fig.4g demonstrates these mechanisms. In general, the resistance of a conductor is derived from the equation: $R = \rho \times L/A$, where ρ , L and A are the resistivity, length and cross-sectional area of the conductor, respectively. Thus, resistance change could be given by $\Delta R/R_0 = (1+2\nu) \varepsilon + \Delta\rho / \rho_0$, where the ν and ε are Poisson's ratio and strain, respectively. According to the equation, the resistance change is dependent on the strain and resistivity, and the resistivity of GnP stays the same after stretch [49]. Thus, the composite film could be used as a strain gauge of flexible strain sensor.

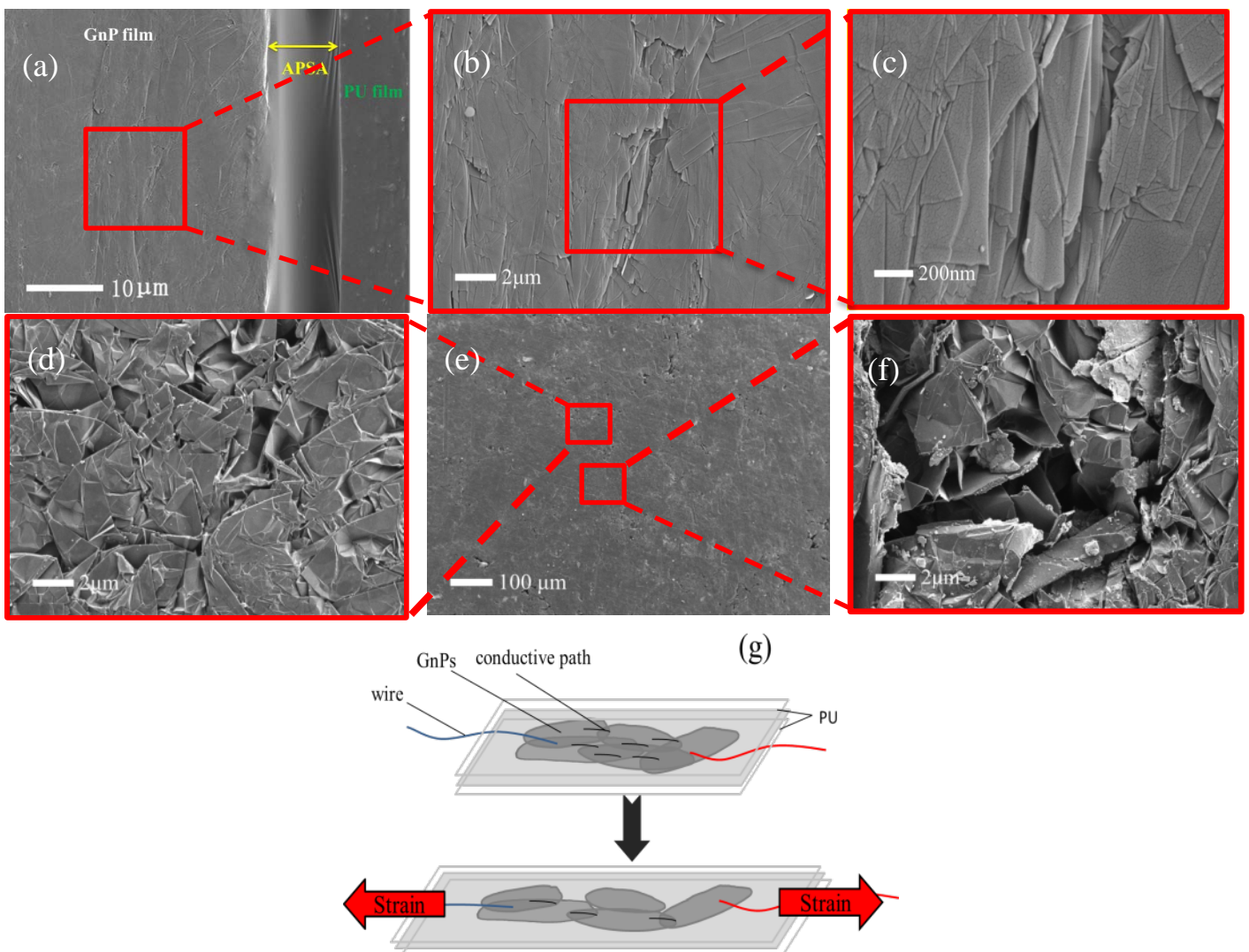


Fig. 4. (a–c) cross-sectional morphology of the composite film; (d–f) surface morphology of the GnP film; (g) schematic of sensor mechanism.

3.3 Mechanical performance

Young's moduli and tensile strengths are measured to investigate the mechanical performance of the composite films. Fig. 5a shows the Young's moduli and tensile strengths of PU film and GnP composite films

with different thicknesses. The thicknesses of the composite films are in range of 0.12–0.2 mm. Obviously, Young’s moduli and tensile strengths are increasing with thickness. *Since the PU films and acrylics pressure-sensitive adhesive (APSA) are identical for all GnP composite films while the weight of GnP is variable (Table 1), the improvement in mechanical properties is due to GnP’s content; the larger thickness of GnP composite film is, the higher GnP’s content is. The enhancement of strength and moduli of PU/GnP composite films are owing to the increase of the rigid and high strength phase (GnPs) in the composite. This is confirmed when comparing the results of samples 2–5 (thickness range 0.12–0.2mm) which contain GnPs to sample 1 (thickness 0.1 mm) with no GnPs.* It also indicates that the thicker films have stronger overlapped structure. Fig. 5b shows the flexibility of the composite film of thickness 0.17 mm in which the composite film was bended into different angles, the resistance increases with angles, however the composite film still shows excellent electrical conductivity.

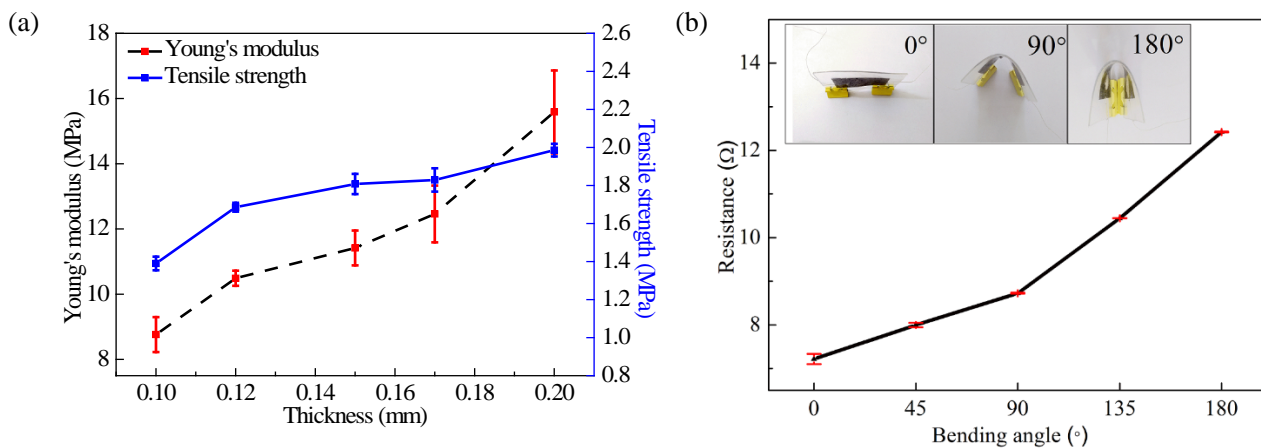


Fig.5. (a) Young’s moduli and tensile strength of GnP composite films with different thickness; (b) the flexibility of a 0.17mm-thickness composite film.

3.4 Sensitivity of strain sensor

Sensitivity is the key property for a strain sensor, which affects the performance of strain sensor directly [9]. Therefore, the gauge factor (GF) was employed to investigate the sensitivity of the strain sensor. Four GnP composite films with different thicknesses were examined to obtain their GF. Fig. 6a is the schematic of GF testing in which the electrical resistance was measured when the tensile test was performing. Fig. 6b is fixture diagram of tensile machine. Fig. 6c shows the relationship between electrical resistance changes and tensile strain of GnP composite films with different thicknesses. The result shows the electrical resistance increases with strain due to the mechanisms discussed in the section 3.2. Furthermore, the change in resistance

(ΔR) decreases with the composite film thickness at same strain. By contrast, the black curve (0.12 mm) shows the highest (ΔR) among all other curves at same strain range in Fig. 6c, while it is less linear with some fluctuations which could be caused by structural instability of thinner film, suggesting fewer GnPs overlaps in the thickness direction and more micro-sized cracks. The other three curves show stable increase and the green curve (0.20 mm) is most stable. In addition, the measurement range increases with thickness and the 0.17 mm and 0.20 mm-thick films have wide measurement range of 0%-25%. Fig. 6d is the GF calculated by the result in Fig. 6c. In summary, the film with 0.12 mm thickness shows highest gauge factor but lowest linearity and smallest measurement range. The other films show better linearity and stable increased resistance. *Therefore, based on both mechanical performance test and GF measurement, we chose the composite film with 0.17 mm thickness to fabricate the flexible strain sensor as the object of the following study.*

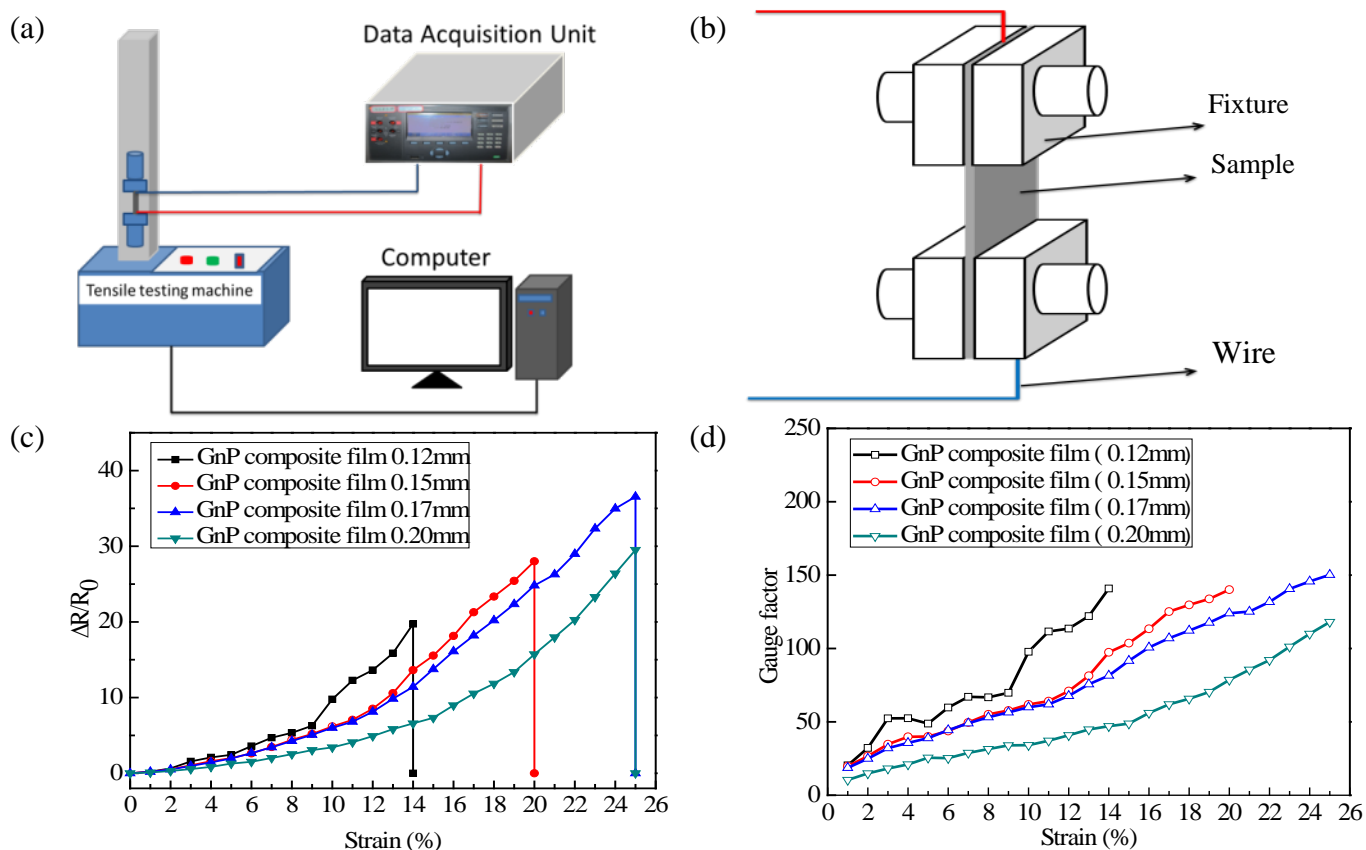


Fig. 6. (a) the schematic of gauge factor testing; (b) the fixture schematic of tensile machine; (c) The curve of resistance changes and strain; (d) the curves of gauge factor and strain.

3.5 Sensitivity of strain sensor

We then conducted cyclic tensile testing to study the stability and reproducibility of the strain sensor. The result exhibits good durability after 1000 cycles at 5% in Fig. 7a, the resistance changes of first 10 cycles

and last 10 cycles are compared and we found the waveform is roughly same, indicating the sensor has good stability and reproducibility thanks to the good elasticity of PU film and strong adhesion of the acrylics pressure-sensitive adhesive. Besides, a response time testing of the strain sensor was conducted and the result was shown in Fig. 7b; the strain sensor responds instantaneously to cyclic loading. We measured the response time when the strain sensor was applied 10% strain; it is 70 ms, indicating the flexible sensor has quick response ability. A good sensor requires not only high sensitivity but also good stability and quick response ability. Obviously, our sensor meets these requirements.

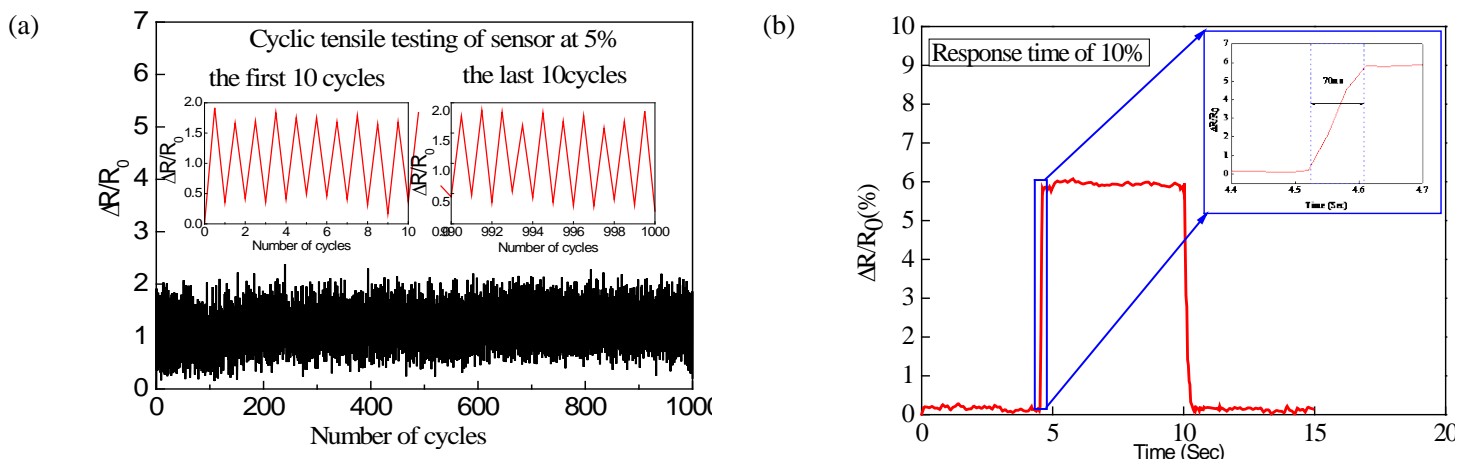


Fig. 7. (a) The result of cyclic tensile testing of the sensor at 5%; (b) the response time testing of the sensor at 10%. *0.17-thickness strain sensor was used for all measurement.*

3.5 Sensor application

As discussed in previously, to be applied as wearable device for body motion measurement, the strain sensor needs to be flexible, highly sensitive, and light in weight [17, 50]. In this study, five typical body motions for wearable device including pulse, finger, cheek, forearm muscle movements, and human vocalization were investigated.

Fig. 8 shows the flexible strain sensor used to monitor real-time pulse movement. Fig. 8a is the schematic of pulse movement measurement and the sensor was glued on the skin region where pulse movement is strongest. A photograph of the sensor was given in which the black part is GnP film and the transparent part is PU film. The pulse of an adult male's in the normal condition is around 12-13 beats per 10 seconds. The results recorded by our strain sensor accurately reflect the pulse movement of a healthy adult clearly (Fig. 8b).

And the sensor achieves stable pulse movement monitoring. In order to amplify the pulse signal and remove undesirable noise over faint pulse signal, we measured pulse movement again and used a 0.5 Hz-10 Hz band-pass filter on MATLAB at same time to filtrate the ambient noise. Fig. 8c gives the comparison between the pulse waveforms before filter and after filter. The pulse waveform measured by our strain sensor highly agrees with the standard pulse waveform in Fig.8d, even the percussion wave and the descending limb wave was observed [51, 52]. It is well known that pulse waveform signal is an important auxiliary parameter to examine whether the arterial blood vessels are normal. It can be used to predict hypertension, coronary heart disease and other diseases, especially in hospital settings [53-55]. Therefore, our GnP composite films can be used as wearable device to monitor pulse movement for predicting body health.

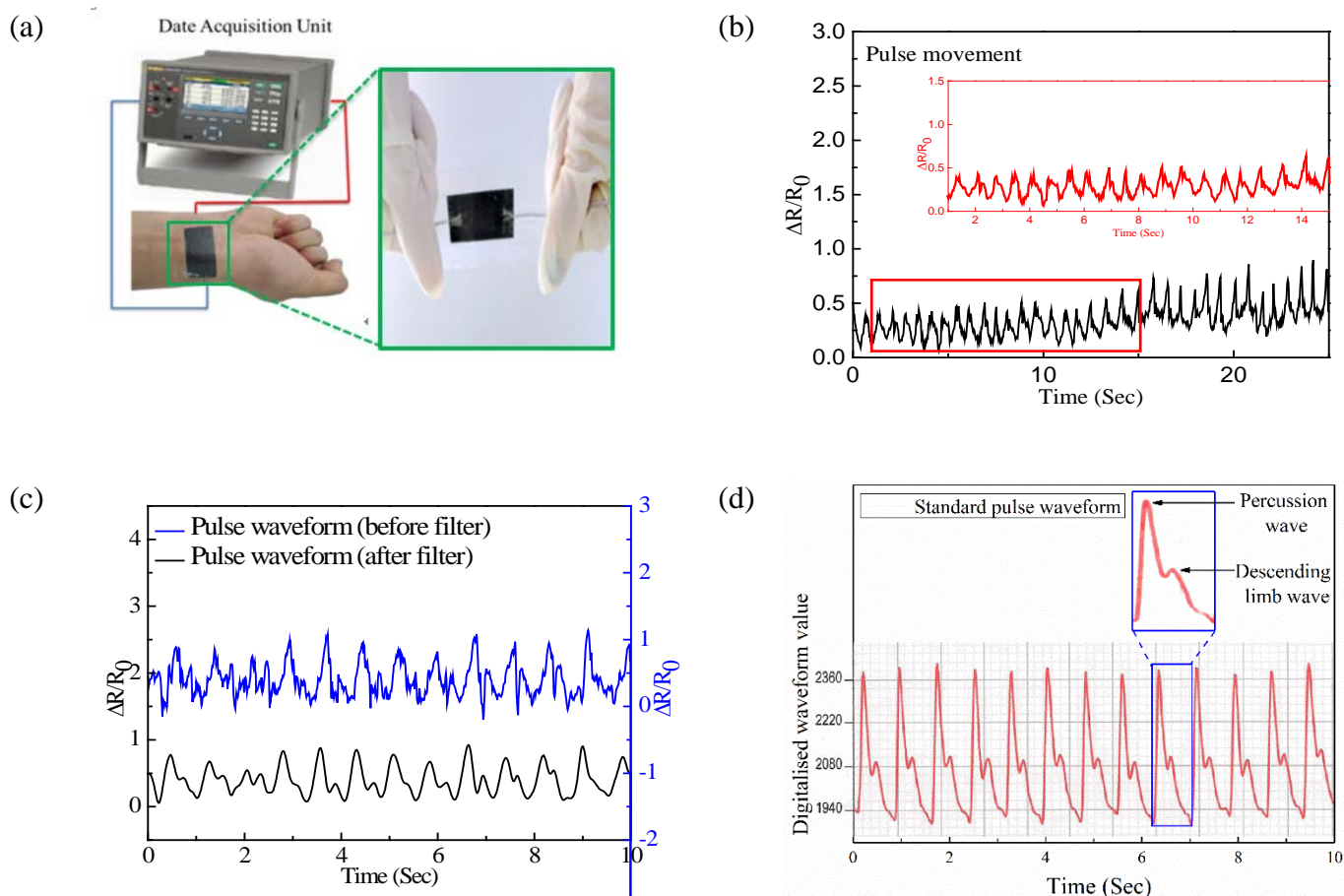


Fig. 8. (a) Schematic of pulse movement measurement and photographs of the strain sensor; (b) the result of real-time monitoring for pulse movement; (c) pulse waveform contrast between before filter and after filter; (d) the standard pulse waveform. *0.17-thickness strain sensor was used for all measurement.*

Fig. 9a shows the strain sensor recorded the behavioral changes when the fingers were repeatedly bended. The strain sensor was attached tightly on a finger in straight state; the resistance of the sensor nearly remains

constant with slight fluctuation. When the finger starts bending, the sensor would be stretched resulting in a sharp increase of resistance. Once the finger moves back to its original position, the resistance recovers instantly due to elasticity of the sensor. Meanwhile, the change of electrical resistance increases with the degree of finger bending motion.

In order to further check the wearable application of our sensor, another two subtle body motions were measured. Fig. 9b&c show the sensor used to monitor forearm muscle and cheek movement caused by muscle deformation. As is shown in Fig. 9b, the sensor was glued on forearm, when we clench, the brachioradialis would contract and cause a deformation perpendicular to the direction of the arm, forming a resistance change signal of the strain sensor. In Fig. 9b, the peak corresponds to the clenching. The resistance of the sensor recovers with opening of the palm.

We proceeded to sense facial muscle movement, because facial expression recognition is vital for the development of human monitoring techniques. Fig. 9c shows the strain sensor used to monitor cheek movement, which is a subtle body movement caused by risorius muscle deformation. There are two peaks corresponding to the bulge movement of cheek skin due to blowing. The left picture in Fig. 9c shows cheek in still state, resistance of the strain sensor keeps stable. The right one is the cheek in movement state. When mouth is blowing, the resistance change reaches peak. This result indicates that our sensor has potential to monitor human facial emotion.

Human vocalization is based on muscle movement and vibration, the sensor was attached onto the throat to identify various pronouncing of English words. The result in Fig. 9d indicates that each signal curve of a word is apparently different to others, and similar to the wave shape of corresponding word, which provides evidence that our sensor can be used for voice recognition.

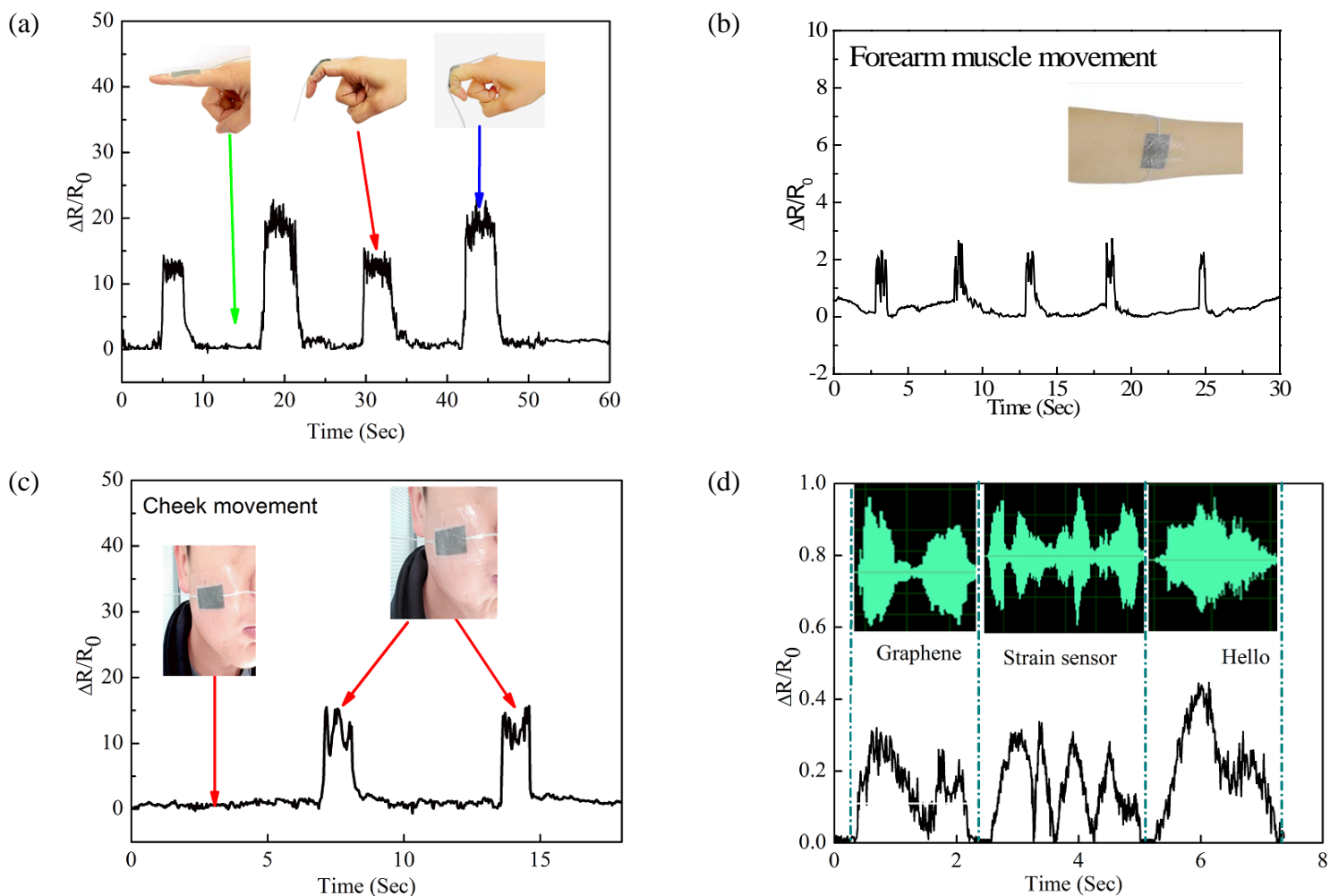


Fig. 9. *0.17-thickness strain sensor* used to monitor (a) finger-bend movement, (b) forearm muscle movement, (c) cheek movement, and (d) voice vibration

3.6 Temperature-response and pressure-response

Temperature has influence on electrical conductivity and GF is temperature dependent [56, 57]. The resistance change caused by temperature is called temperature drift. The electrical resistance of the strain sensor was measured over a temperature range of 20–150 °C to study the temperature response.

Fig. 10 shows the temperature-resistance curve. The resistance does not change significantly under 100°C, while it increases sharply above 100°C with more distinct error. According to the result, the strain sensor's appropriate operating temperature *range is* 20-100°C, temperature drift of the strain sensor in this range is too tiny to consider. *On the other hand, resistance changes obviously when sensor temperature is beyond 100°C. this is because the isotropic conductive adhesive (ICA) start to lose its binding strength to the GnP film; the*

glass transition temperature of ICA is $\sim 90^{\circ}\text{C}$ [58]. This would increase the electrical resistance at the interface between GnP film and ICA, and ICA with the copper wires which consequently increases the overall electrical resistance of the strain sensor. The viscous state of ICA explains the high standard deviation attained at temperature $>100^{\circ}\text{C}$.

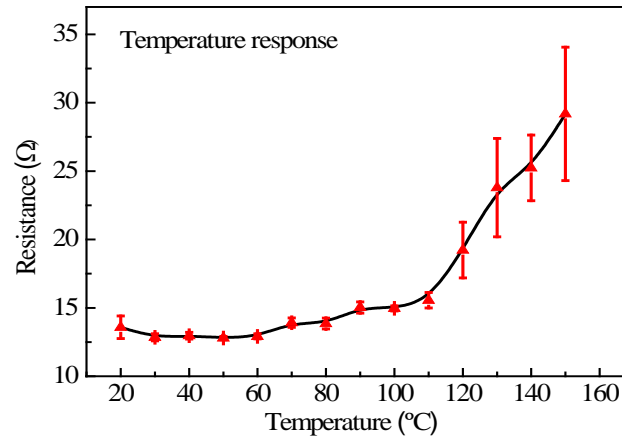


Fig. 10. Temperature response of *0.17-thickness sensor*

To evaluate the pressure response of the strain sensor, different levels of pressure were given to measure the electrical resistance of the strain sensor. Fig. 11 shows the resistance of the strain sensor under pressure ranging from 0 to 1 MPa. The electrical resistance of the strain sensor decreases with the pressure, possibly due to the decrease in the inter-particle distance and increase in GnP sheets connection and overlaps. The pressures on skin surface during body motions are generally not more than 10 kPa. For example, the pressure on skin surface of normal pulse movement is 5.33 kPa. The electrical resistance changes of the strain sensor under 10 kPa pressures is too tiny to observe. Thus, the resistance changes are mainly caused by strain in the sensor application as wearable device in this work. Besides, In Fig. 11, the sharpest decline is between 200 kPa and 600 kPa, therefore the sensor could be used as a pressure sensor in the operating range of 200-600 kPa.

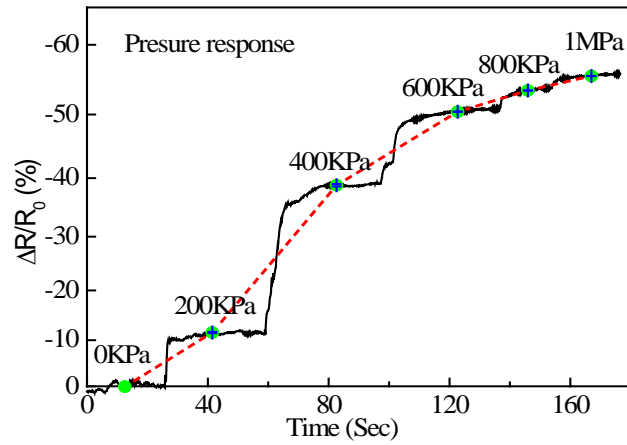


Fig. 11. Resistance change of strain sensor of *0.17-thickness sensor* at different pressures.

We have compared our PU/GnP flexible strain sensor with reported flexible strain sensors in terms of thickness, stretch ability, fabrication/difficulty, electrical conductivity and wearable ability (Table 2). In contrast with the previously demonstrated flexible strain sensor, our strain sensor based on PU/GnP exhibits various advantages, including (1) higher level of electrical conductivity (1430 S/cm), (2) high sensitivity (GF), (3) facile and cost-effective approach of fabrication and (4) reliable bio-signal measurement. The GF of flexible strain sensor in this work is 255.45% higher than the strain sensor based on Polydimethylsiloxane (PDMS)/graphene, 72.69% higher than PU core/ Graphene, and 89.87% higher than Electro spun mats / RGO, respectively. High GF enables the strain sensor to detect the slight movement such as pulse movement accurately. In this work, we measured five bio-signals to study the wearable ability of our strain sensor. As shown our strain sensor has greater potential to be used as wearable device because it has the ability to monitor both large and slight, low and high- frequency movement.

Table 2. Comparison of flexible strain sensors fabricated by different materials

Substrate/filler	Thickness (mm)	Fabrication /difficulty	Stretch ability	Electrical conductivity (S/cm)	Gauge factor	Wearable ability	Ref.
PU/MWCNTs	1.6	3D print ★★★	100%	0.01	176	+	[24]
PDMS/Graphene	0.12	Spraying ★★	20%	0.42	42.2	++	[59]
PU/ PAN electro spun mats	0.1-0.2	Polymerization ★★★	110%	0.43	17.15	+	[60]
PU core/Graphene	0.2	Coating ★★★	50%	0.015	86.86	+	[46]
Electro spun mats/ RGO	0.2	Polymerization ★★	250%	0.002	79	+++	[61]
PU/GnP	0.12-0.20	LBL laminating ★	25%	1430±50	150	+++++	This work

* PDMS (Polydimethylsiloxane), PAN (Polyaniline), LBL (Layer by layer), RGO (Reduced graphene oxide),

* The number of “★” means the difficulty of corresponding fabrication which is measured by the fabrication time and process; one ★ is the lowest

* The number of “+” means the number of the bio-signals measured in the paper.

Conclusion:

In summary, we developed a highly sensitive and flexible strain sensor based on PU/GnP composite film fabricated by a facile approach. The flexible strain sensor was fabricated via layer by layer laminating method which is simple and cost-effective. The PU substrate gives the strain sensor good flexibility and stretch ability (up to 25%). The strain gauge made of GnP composite film achieves excellent electrical conductivity and high GF of 150, which is higher than the similar sensors reported. The cyclic tensile test shows our strain sensor has good stability and reproducibility after 1000 cyclic tensile test at 5% strain. For sensor applications, the flexible strain sensor successfully achieves accuracy monitoring for 5 body motions covering both large and slight, low and high- frequency movement, thus it has good potential for wearable device. In addition, the strain sensor has low temperature drift in the operating temperature range of 0-100°C, it has the ability of working in most condition of wearable device. According to the pressure response test of the strain sensor, the resistance changes are not influenced by pressure when the strain sensor was used as wearable device. Finally, we made a multifaceted comparison of different flexible strain sensors and summarized four

advantages of our strain sensor including (1) high sensitivity (GF), (2) facile fabrication approach, and (3) various applications in wearable device.

Acknowledgement

QM and ZL thank Asbury and Huntsman (Melbourne) for providing the graphite intercalation compounds (1721 and 1395) and Jeffamine D 400, respectively. This work was financially supported by the Natural Science Foundation of Liaoning Province (20170520142). Dr. Tianqing Liu is supported by NHMRC Early Career Fellowship (1112258).

Conflicts of interest

All authors declare that they have no conflict of interest.

References:

- [1] S-H Bae, Y Lee, BK Sharma, H-J Lee, J-H Kim, J-H Ahn (2013) Carbon 51: 236.
Doi:10.1016/j.carbon.2012.08.048
- [2] T Yamada, Y Hayamizu, Y Yamamoto, et al. (2011) Nat Nanotechnol 6: 296. Doi:10.1038/nnano.2011.36
- [3] G Yu, J Hu, J Tan, Y Gao, Y Lu, F Xuan (2018) Nanotechnology 29: 115502. Doi:10.1088/1361-6528/aaa855
- [4] A Sakhaee-Pour, MT Ahmadian, A Vafai (2008) Solid State Communications 147: 336.
- [5] R Moriche, M Sánchez, A Jiménez-Suárez, SG Prolongo, A Ureña (2016) Composites Science & Technology 123: 65.
- [6] T Yang, X Jiang, Y Zhong, et al. (2017) ACS sensors 2: 967. Doi:10.1021/acssensors.7b00230
- [7] Y Liu, M Pharr, GA Salvatore (2017) ACS Nano 11: 9614. Doi:10.1021/acsnano.7b04898
- [8] Y Pang, H Tian, L Tao, et al. (2016) ACS Appl Mater Interfaces 8: 26458. Doi:10.1021/acsami.6b08172
- [9] JJ Park, WJ Hyun, SC Mun, YT Park, OO Park (2015) ACS Appl Mater Interfaces 7: 6317.
Doi:10.1021/acsami.5b00695
- [10] Y Wang, L Wang, T Yang, et al. (2014) Advanced Functional Materials 24: 4666.
Doi:10.1002/adfm.201400379
- [11] JW Zha, B Zhang, RKY Li, ZM Dang (2016) Composites Science & Technology 123: 32.
- [12] R Moriche, A Jiménez-Suárez, M Sánchez, SG Prolongo, A Ureña (2017) Composites Science & Technology 146: 59.
- [13] CJ Lee, S Jun, BK Ju, JW Kim (2017) Physica B Condensed Matter 514: 8.
- [14] MD Ho, Y Ling, LW Yap, et al. (2017) Advanced Functional Materials 27: 1700845.

- [15] S Liu, Y Lin, Y Wei, S Chen, J Zhu, L Liu (2017) *Composites Science & Technology* 146: 110.
- [16] Y Zheng, Y Li, K Dai, et al. (2018) *Composites Science & Technology* 156: 276.
- [17] Z Zhan, R Lin, VT Tran, et al. (2017) *ACS Appl Mater Interfaces* 9: 37921. Doi:10.1021/acsami.7b10820
- [18] W Huang, K Dai, Y Zhai, et al. (2017) *ACS Appl Mater Interfaces* 9: 42266. Doi:10.1021/acsami.7b16975
- [19] S Araby, Q Meng, L Zhang, et al. (2014) *Polymer* 55: 201. Doi:<https://doi.org/10.1016/j.polymer.2013.11.032>
- [20] Y Yan, M Potts, Z Jiang, V Sencadas (2018) *Composites Science & Technology* 162: 14.
- [21] B Hao, L Mu, Q Ma, S Yang, PC Ma (2018) *Composites Science & Technology* 163: 162.
- [22] B Nie, X Li, J Shao, et al. (2017) *ACS Appl Mater Interfaces* 9: 40681. Doi:10.1021/acsami.7b12987
- [23] S Zhang, H Zhang, G Yao, et al. (2015) *Journal of Alloys and Compounds* 652: 48.
Doi:10.1016/j.jallcom.2015.08.187
- [24] JF Christ, N Aliheidari, A Ameli, P Pötschke (2017) *Materials & Design* 131: 394.
Doi:10.1016/j.matdes.2017.06.011
- [25] AK Geim (2009) *Science* 324: 1530. Doi:10.1126/science.1158877
- [26] N Materials (2007) *Nature Material* 6: 183.
- [27] F Banhart, J Kotakoski, AV Krasheninnikov (2011) *ACS Nano* 5: 26. Doi:10.1021/nn102598m
- [28] JR Potts, DR Dreyer, CW Bielawski, RS Ruoff (2011) *Polymer* 52: 5. Doi:10.1016/j.polymer.2010.11.042
- [29] Y Zhu, S Murali, W Cai, et al. (2010) 22: 3906. Doi:10.1002/adma.201001068
- [30] I Zaman, HC Kuan, Q Meng, et al. (2012) *Advanced Functional Materials* 22: 2735.
- [31] J Ma, Q Meng, I Zaman, et al. (2014) *Composites Science & Technology* 91: 82.
- [32] G Shi, S Araby, CT Gibson, Q Meng, S Zhu, J Ma (2018) *Advanced Functional Materials*: 1706705.
- [33] Q Meng, H Wu, Z Zhao, S Araby, S Lu, J Ma (2017) *Composites Part A Applied Science & Manufacturing* 92: 42.
- [34] S Araby, N Saber, X Ma, et al. (2015) *Materials & Design (1980-2015)* 65: 690.
Doi:<https://doi.org/10.1016/j.matdes.2014.09.069>
- [35] S Araby, L Zhang, H-C Kuan, J-B Dai, P Majewski, J Ma (2013) *Polymer* 54: 3663.
Doi:<https://doi.org/10.1016/j.polymer.2013.05.014>
- [36] C-F Cao, G-D Zhang, L Zhao, et al. (2019) *Composites Science and Technology* 171: 162.
Doi:<https://doi.org/10.1016/j.compscitech.2018.12.014>

- [37] F Qiang, L-L Hu, L-X Gong, L Zhao, S-N Li, L-C Tang (2018) *Chemical Engineering Journal* 334: 2154.
Doi:<https://doi.org/10.1016/j.cej.2017.11.054>
- [38] Y-J Tan, J Li, Y-F Chen, et al. (2019) *Polymer Testing* 75: 142.
Doi:<https://doi.org/10.1016/j.polymertesting.2019.02.004>
- [39] J-H Cai, Y-F Chen, J Li, et al. (2019) *Chemical Engineering Journal* 370: 176.
Doi:<https://doi.org/10.1016/j.cej.2019.03.223>
- [40] H Xu, Y Li, N-J Huang, et al. (2019) *Journal of Hazardous Materials* 363: 286.
Doi:<https://doi.org/10.1016/j.jhazmat.2018.09.082>
- [41] Q Wu, L-X Gong, Y Li, et al. (2018) *ACS Nano* 12: 416. Doi:10.1021/acsnano.7b06590
- [42] M Wang, K Zhang, X-X Dai, et al. (2017) *Nanoscale* 9: 11017. Doi:10.1039/C7NR02322G
- [43] F Qiang, S-W Dai, L Zhao, et al. (2019) *Sensors and Actuators B: Chemical* 285: 254.
Doi:<https://doi.org/10.1016/j.snb.2019.01.043>
- [44] I Zaman, HC Kuan, J Dai, et al. (2012) *Nanoscale* 4: 4578. Doi:10.1039/c2nr30837a
- [45] M Qingshi, J Jian, W Ruoyu, et al. (2014) *Nanotechnology* 25: 125707.
- [46] X Li, T Hua, B Xu (2017) *Carbon* 118: 686. Doi:10.1016/j.carbon.2017.04.002
- [47] J Ma, Q Meng, A Michelmore, et al. (2013) *Journal of Materials Chemistry A* 1: 4255.
- [48] G Shi, Z Zhao, J-H Pai, et al. (2016) *Advanced Functional Materials* 26: 7614. Doi:10.1002/adfm.201602619
- [49] A Nakamura, T Hamanishi, S Kawakami, M Takeda (2017) *Materials Science and Engineering: B* 219: 20.
Doi:10.1016/j.mseb.2017.02.012
- [50] S Ryu, P Lee, JB Chou, et al. (2015) *ACS Nano* 9: 5929. Doi:10.1021/acsnano.5b00599
- [51] IB Wilkinson, IR Hall, H MacCallum, et al. (2002) *Arteriosclerosis, thrombosis, and vascular biology* 22: 147.
- [52] LM Bortel, Van, L Stephane, B Pierre, et al. (2012) *Journal of Hypertension* 30: 445.
- [53] W Xuewen, G Yang, X Zuoping, C Zheng, Z Ting (2014) *Advanced Materials* 26: 1336.
- [54] MF O'Rourke, A Pauca, XJ Jiang (2001) *Br J Clin Pharmacol* 51: 507.
- [55] HC Koydemir, A Ozcan (2018) *Annu Rev Anal Chem (Palo Alto Calif)* 11: 127. Doi:10.1146/annurev-anchem-061417-125956
- [56] S Sayed, M Gamil, AMR Fath El-Bab, AAEM Abd Elmoneim (2015) *Key Engineering Materials* 644: 115.
- [57] DI Bower (1972) *Journal of Physics E: Scientific Instruments* 5: 846. Doi:10.1088/0022-3735/5/9/002

- [58] MJ Yim, KWJEML Paik (2006) 2: 183.
- [59] S Chun, Y Choi, W Park (2017) Carbon 116: 753. Doi:10.1016/j.carbon.2017.02.058
- [60] M Tian, Y Wang, L Qu, et al. (2016) Synthetic Metals 219: 11. Doi:10.1016/j.synthmet.2016.05.005
- [61] Y Wang, J Hao, Z Huang, et al. (2018) Carbon 126: 360. Doi:10.1016/j.carbon.2017.10.034